Quasicrystalline Weyl points and densely distributed Fermi–Bragg arcs

André Grossi e Fonseca,[1] Thomas Christensen,[1] John D. Joannopoulos,[1] and Marin Soljačić[1]

[1]*Department of Physics, Massachusetts Institute of Technology, Cambridge, Massachusetts 02139, USA*

We propose a general mechanism for obtaining Weyl points in a stack of 2D quasicrystals by interpolating the Hamiltonian between two topologically distinct phases, with the interpolating parameter the crystal momentum in the periodic direction. To illustrate our idea, we study an interpolated version of the Qi–Wu–Zhang model defined on a Penrose quasicrystal. We acertain the existence of two Weyl points of opposite chiralities through the local Chern marker, a real-space version of the Chern number, as well as the density of states. We also uncover novel surface states we dub Fermi–Bragg arcs, due to their intimate relationship to the diffraction spectrum. Our theory is general and can be readily extended to aperiodic systems. We also discuss the possibility of this mechanism explaining recently observed 3D band crossings in a stack of chalcogenide quasicrystals, as well as direct experimental realizations of the model.

Topological band theory has become a well-established tool for understanding robust physical phenomena in both quantum [1, 2] and classical [3–6] systems. One of its earliest successes was in justifying the precise quantization of the Hall resistivity of a 2D electron gas in the quantum Hall effect [7], through a topological invariant, the Chern number [8]. With the subsequent prediction [9] and discovery [10] of topological insulators, a whole slew of topological quantum numbers were uncovered, which characterize the topology of a band and lead to scatter-free propagating edge states through the bulk-boundary correspondence.

Although topological band theory was originally elaborated to deal with gapped systems, its purview has been successfully extended to many gapless phenomena. A prominent example is in the context of Weyl points (WPs), 3D band crossings that act as monopoles of Berry curvature in crystal-momentum space with well-defined chirality [11]. Since their simultaneous discovery in TaAs [12] and double gyroid photonic crystals [13], WPs have been intensely investigated due to their fundamental connection to high-energy physics [14], unusual surface states known as Fermi arcs [12, 13, 15], and unique optical responses [16].

Another apparent limitation of topological band theory is its reliance on discrete translational invariance, which is absent in quasicrystalline, amorphous and disordered systems. However, real-space methods to detect nontrivial topology were subsequently developed [17–19], leading to the prediction of topological states in systems for which Bloch's theorem breaks down [20, 21]. To this day, systematically diagnosing the topology while bypassing any reference to k-space remains a lively frontier [22]. In addition to expanding the scope of topology, this represented a major conceptual step in understanding the minimal ingredients for the existence of topologically protected modes.

In this Letter, we combine these two domains by presenting a general mechanism for obtaining Weyl physics in a stack of non-crystalline systems. Our idea is to interpolate an aperiodic 2D Hamiltonian between two distinct topological phases through a third periodic coordinate (here, z). Because a system can only undergo a topological phase transition through gap closure (assuming any symmetries protecting the topology to be unbroken), the interpolation leads to WPs in the spectrum at those points in the z Brillouin zone (zBZ) where the topological invariant changes. Focusing on the quasicrystalline case, we illustrate our idea through a tight-binding Hamiltonian defined on a Penrose tiling [23], which we show to be associated with WPs through signatures in the topological phase diagram and density of states (DOS), as well as a novel kind of surface states we call *Fermi–Bragg arcs* due to their connection with the diffraction spectrum. Finally, we discuss the model in real space and experimental relevance, both as a possible mechanism behind the recently observed band crossings in a stack of chalcogenide quasicrystals [24], as well as its direct realization.

Model and topological marker. We start by defining a lattice for the tight-binding model, which we take to be the vertices of the Penrose quasicrystal, a small section of which is shown in Fig. 1(a), along with the hopping parameters of Eq. (1). Because we employ both open and periodic boundary conditions (O/PBC), we construct the lattice through Penrose tiling approximants [25], finite supercells of increasing order n that systematically approximate the Penrose quasicrystal as $n \to \infty$ while restricting the number of defects (i.e., an edge at which the matching rules are violated) to two per unit cell. The number of vertices at order n is $N = F_{2n+3} + F_{2n+5}$, where F_n is the nth Fibonacci number [26] (see Supplemental Material for details of the tiling approximant construction).

We then consider the Qi–Wu–Zhang (QWZ) model [27], a two-band model of a Chern insulator whose generalized version in real space reads

$$\begin{aligned} H_{\mathrm{QWZ}}(M) &= t \sum_{\boldsymbol{R}\boldsymbol{a}\alpha\beta} T_{\alpha\beta,\boldsymbol{a}} c^{\dagger}_{\boldsymbol{R},\alpha} c_{\boldsymbol{R}+\boldsymbol{a},\beta}, \\ T_{\alpha\beta,\boldsymbol{0}} &= (2+M)\sigma_z, \quad T_{\alpha\beta,\boldsymbol{a}} = \frac{1}{2}\begin{pmatrix} -1 & i\,e^{-i\theta_a} \\ i\,e^{i\theta_a} & 1 \end{pmatrix}, \end{aligned} \tag{1}$$

where t is the hopping amplitude, the sum runs over all sites $\boldsymbol{R}$ at the vertices of the Penrose quasicrystal, local orbitals (taken to be s and p as in Fig. 1(b)) are denoted by Greek letters, $\boldsymbol{a}$ labels neighbors connected to $\boldsymbol{R}$ by a rhombus edge (and $\boldsymbol{a} = \boldsymbol{0}$ corresponds to the on-site potential), θ_a is the angle of the edge $\boldsymbol{a}$ with the x axis, and M is a mass parameter controlling the topological phase. On a square lattice, this model undergoes topological phase transitions at $M = -4, -2$ and 0. In particular, the Chern number C changes from -1 to 0 when M changes sign from negative to positive. Because

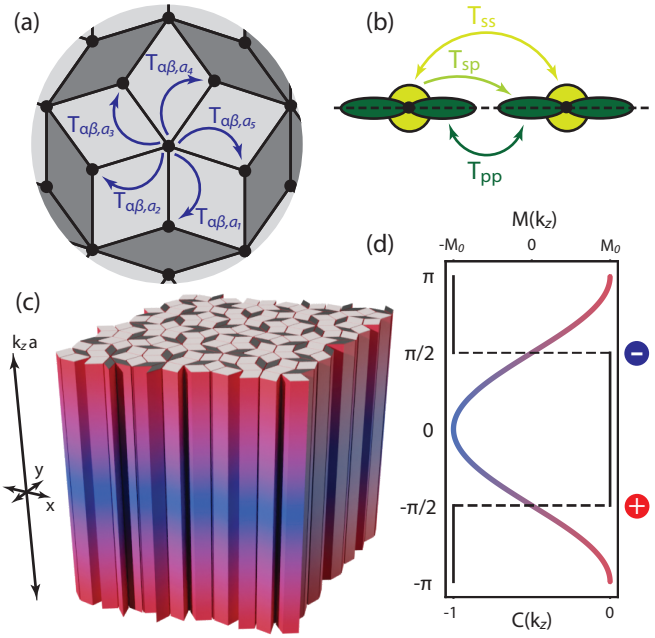

Figure 1. Mechanism for Weyl points in a quasicrystal stack. (a) Top view of a small section of a Penrose quasicrystal, with fat and skinny rhombuses in light and dark grey, respectively. Excitations can hop to sites connected by a bond, with amplitudes $T_{\alpha\beta,a}$ given by Eq. (1). Here, nearest neighbors are $a_i = (\sin 2\pi j/5, \cos 2\pi j/5)a$, $j = 1, ..., 5$ and a the bond length. Throughout this figure, double-sided/one-sided arrows indicate direction independent/dependent hoppings. (b) Side view of lattice, with s and p orbitals in yellow and green, respectively. Inter- and intra-orbital hopping matrix elements are indicated. (c) 3D extension of 2D model [Eq. (4)], with the mass parameter M a sinusoidal function of k_z, with different values indicated by color gradient. (d) Mass parameter and expected Chern number C as a function of k_z. When M changes sign, C jumps discontinually, indicating a gap closure. Weyl points are represented by colored spheres, with signs indicating the chirality.

Eq. (1) bears no reference to crystallinity, it can be readily employed in an aperiodic system.

In order to compute $C(M)$ for a quasicrystal, one cannot integrate the Berry curvature, as k_x and k_y are not good quantum numbers. This issue is circumvented by applying the formalism of the local Chern marker [17], which is defined at each lattice site i as

$$C_i = -\frac{4\pi}{\Omega}\,\mathrm{Im}\Big[\sum_j \langle i|\, x_Q\,|j\rangle\,\langle j|\, y_P\,|i\rangle\Big], \tag{2a}$$

with

$$\langle i|\, x_Q\,|j\rangle = \sum_k Q_{ik}x_k P_{kj}, \quad \langle j|\, y_P\,|i\rangle = \sum_k P_{jk}y_k Q_{ki}, \tag{2b}$$

$$P = \sum_{\epsilon_\lambda<\epsilon_F} |\psi_\lambda\rangle\langle\psi_\lambda|, \qquad Q = 1 - P, \tag{2c}$$

and Ω the unit cell area, which for the Penrose quasicrystal we take to be the weighted average of the two rhombus areas (see Supplemental Material).

The local Chern marker functions as a Chern density, in the sense that, in the thermodynamic limit, its average over the sample converges to the usual Chern number. It has also been shown to have properties akin to a local order parameter near criticality [28, 29] and was recently directly measured in an ultracold bosonic system [30]. Although for a finite system the average of Eq. (2a) over all lattice sites vanishes, its bulk value is well quantized (see Supplemental Material). In order to assign a global index to the system, one can compute an averaged local Chern marker

$$C_D(R) = \frac{1}{N}\sum_{i\in D} C_i, \tag{3}$$

where the average is performed over N points in the disk D with radius R. In practice, R is chosen large enough to avoid microscopic fluctuations but small enough to be restricted to the bulk [31].

To illustrate our general mechanism, we now propose a 3D version of the QWZ model we call the interpolated QWZ (iQWZ) model

$$H_{\mathrm{iQWZ}}(k_z) = H_{\mathrm{QWZ}}(M_0 \cos k_z a), \tag{4}$$

where a is the bond length. A heuristic depiction of this model is given in Fig. 1(c). The periodic dependence on k_z defines a zBZ and implies real-space periodicity along z with simple interlayer hopping, as we shall see later. One can then compute C_D at different values of k_z. Variations of the mass parameter and the expected phase diagram of this model are shown in figure 1d, and we anticipate a pair of WPs at $k_z a = \pm\pi/2$ with opposite chiralities [32]

$$\chi_\pm = \lim_{k_z\to\pm\pi/2^+} C(k_z) - \lim_{k_z\to\pm\pi/2^-} C(k_z) = \mp 1, \tag{5}$$

as required by the Nielsen-Ninomyia theorem [33, 34]. Henceforth, we set $M_0 = 1$, although it could serve as an additional experimental knob in a realization of our model.

Bulk signatures. Fig. 2 depicts numerical evidence of the presence of WPs through bulk observables. For each value of k_z, the model leads to two bands, with states filling the gap if $|k_z a| < \pi/2$. These are chiral edge states stemming from nontrivial topology, which vanish upon imposing PBCs [Fig. 2(a)]. We also compute the projected band structure in Fig. 2(b). The band gap reaches a minimum at $k_z a \approx \pm\pi/2$ but does not fully close due to the system's finite size; but as we show in the Supplemental Material, the band gap asymptotes to zero as the system size increases, yielding linear band touchings in the thermodynamic limit. Also, the topological and trivial phases share a similar band gap, meaning that the WPs are well-isolated and can be tracked through the DOS [Fig. 2(c)]. Despite the finite gap, the DOS is quadratic near $\varepsilon = 0$ to a good approximation, precisely the expected dependence for isolated WPs. Finally, we evaluate C_D as a function of k_z for a fixed averaging radius [Fig. 2(d)], and our results shows excellent agreement with the expected phase diagram. The sudden jumps at the same momenta at which the gap is minimized confirm once again the presence of WPs. Interestingly,

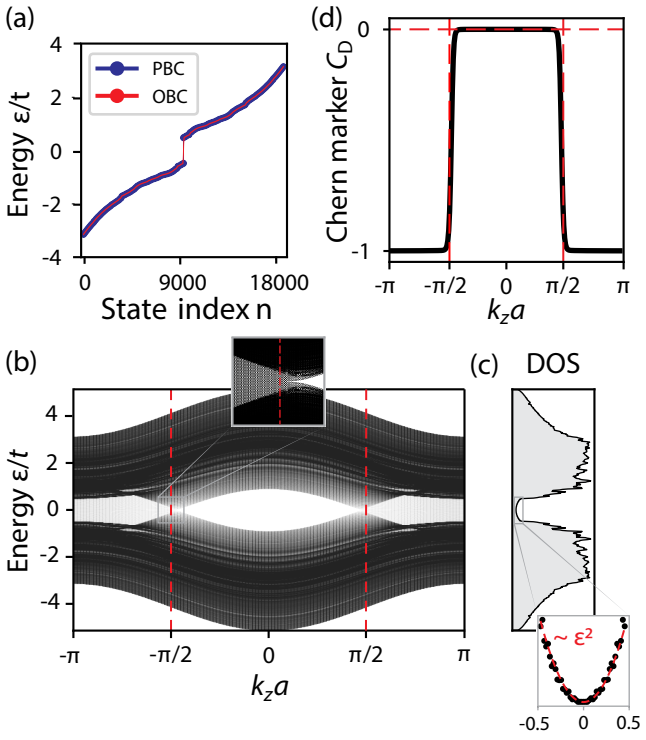

Figure 2. Bulk properties of the iQWZ model. (a) Energy eigenvalues ε as a function of state index n for $k_z a = \pi$. For PBCs, the system has a finite gap, whereas for OBCs mid-gap states appear, signaling non-trivial topology. (b) Projected band structure under OBCs in the zBZ. For $|k_z a| < \pi/2$, the system is gapped, whereas for $|k_z a| > \pi/2$ edge states populate the bulk gap, as shown in the inset. Red dashed lines indicate the gap closing points for a square lattice. (c) Density of states under PBCs, which vanishes at $\varepsilon = 0$ quadratically as shown in inset. Red dashed line indicates a quadratic fit. (d) Averaged Chern marker [Eq. (3)] in the zBZ for $R = 12a$. The step-like behavior near $k_z a \approx \pm\pi/2$, indicates topological phase transitions at these points. (a–c) and (d) were computed using approximants $n = 7$ (9349 sites) and $n = 6$ (3571 sites), respectively.

the gap closure occurs very close to the critical point for a square lattice, suggesting that the topology is, to a large extent, lattice-independent.

Fermi–Bragg arcs. The presence of WPs in a band structure is typically associated with anomalous surface states deemed Fermi arcs (FAs) [15], arc-like structures in the spectral DOS connecting WPs of opposite chirality. Because these arc states are of topological origin, the customary way of depicting them is to impose OBCs along one direction (say, x) while maintaining periodicity along the two others. In this case, FAs live on slices of the BZ parallel to the plane spanned by the two well-defined momenta (in this example, the (k_y, k_z) plane).

In the present system, it is challenging to define a 2D BZ plane to detect FAs, as only k_z is a good quantum number. However, one can still analyze state distributions in Fourier space, which does not rely on discrete translational invariance. Taking Fourier space as our parameter space also allows us to impose OBCs along both in-plane directions, contrary to the usual practice but more natural for a quasicrystal. Since Fourier momentum is not constrained to lie in a BZ, we investigate the putative arcs for arbitrary q_x and q_y. Throughout, we use the letter q to refer to Fourier momentum and k for crystal momentum.

Firstly, we show in Fig. 3(a) that such anomalous states in the gap are present in the topological regime. Focusing on the x boundaries, these modes are exponentially localized at the surface, providing the first evidence for FAs in our platform, despite the in-plane aperiodicity. In Fig. 3(b), we switch our attention to Fourier-Bloch momentum (q, k_z)-space, which displays rich structure. The spectral DOS, evaluated at the x boundaries, exhibits sharp lines between the WPs (here, located at $k_z a = \pi/2, 3\pi/2$), similarly to the expectation for a crystal. Now, however, in addition to being defined in Fourier rather than crystal momentum space, there are *several* such lines of varying intensity, connecting the WPs vertically.

In order to interpret these results, we first draw an analogy with the crystalline case. If plotted in the extended zone scheme, a crystal exhibits many FAs throughout k-space of the same intensity, one per BZ copy. Furthermore, because each BZ contains one Bragg peak (BP), FAs are in one-to-one correspondence with BPs. This motivates us to compare the quasicrystalline arcs with the BPs, for which we find a precise correspondence [Fig. 3(b)]. Namely, if projected to the q_y axis (or q_x, see Supplemental Material), BPs precisely track the FA positions, with some correlation between arc and peak intensities. For this reason, we dub these novel surface states Fermi–Bragg arcs (FBAs), which are inherently quasicrystalline. We conjecture that this relationship holds true for all peaks, not just the brightest ones shown.

Physically, each BP ring, with fivefold rotational symmetry in the case of the Penrose quasicrystal, defines a pseudo-BZ (PBZ) [35–37]. In analogy to the BZ, the PBZ is constructed by bisecting vectors connecting Γ to points in the ring. If we assume that each FBA is associated with a WP pair, folding into the PBZ lands the pair precisely at Γ. Therefore, in terms of the PBZ, the WPs all have zero "pseudo crystal momentum". Interestingly, this is precisely the point in k-space at which the gap closes in the QWZ model defined on a square lattice when M changes sign [27].

Real-space model. The Hamiltonian we employed Eq. (4) is hybrid, insofar as it is defined in real space in the in-plane (quasicrystalline) directions, but in k_z-space along the vertical direction. As we show in the Supplemental Material, by Fourier transforming in z one obtains a periodic stack of 2D quasicrystals with interlayer coupling restricted to intra-orbital hopping, and each layer precisely tuned to the topological critical point ($M = 0$ in the QWZ model), i.e., a stack of Dirac-like quasicrystals. This means that our mechanism could underlie the recently observed 3D band crossings in a stack of $Ta_{1.6}Te$ quasicrystals, each itself displaying 2D band degeneracies [24].

The fact that each layer is precisely tuned to the phase transition point means that the model is fine-tuned. However, as we argue in the Supplemental Material, the relevant physics remains robust to perturbations: allowing arbitrary inter-orbital

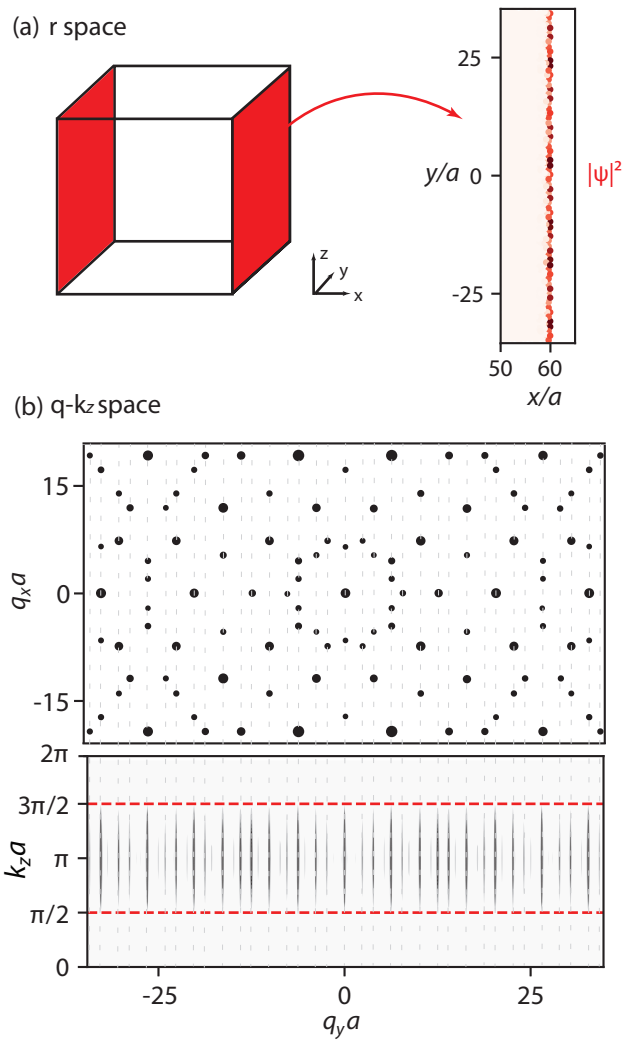

Figure 3. Surface signatures of Weyl points in real and Fourier-Bloch momentum space. (a) Upon imposing OBCs in both x and y and zooming into the x boundary, we observe localized edge modes for values of k_z in the topological regime (edge state shown for $k_z a = \pi$). (b) Structure factor in Fourier space (top, only brightest spots are shown and spot size is proportional to intensity) and spectral DOS at the x boundaries (bottom), with both plots having the same horizontal axis. Vertical dashed lines show that q_y projections of Bragg peaks line up precisely with vertical Fermi arcs, which we therefore refer to as Fermi–Bragg arcs. Horizontal red dashed lines bound the topological region $\pi/2 < k_z a < 3\pi/2$, showing that arcs connect Weyl points of opposite chirality.

mixing has no bearing on the WPs, whereas detuning each layer from the critical point by $\delta M \ll 1$ only shifts them in the zBZ. Therefore, we expect our mechanism to be readily realizable by stacking 2D quasicrystals with Dirac points, on top of some time-reversal breaking mechanism.

Discussion and outlook. In this Letter we have proposed a general mechanism for obtaining 3D level crossings (WPs) in non-crystalline systems by interpolating a 2D topological Hamiltonian between topologically distinct phases, thereby forcing the gap to close. As an example, we studied a suitably parameterized version of the QWZ model, defined on a Penrose quasicrystal. We confirmed the existence of the WPs through the the averaged local Chern marker, a real-space incarnation of the Chern number; the projected band structure, in which the band gap reaches a minimum (and closes for an infinitely sized system) at the expected momenta; the DOS, exhibiting the quadratic dependence typical of isolated WPs; and, surprisingly, a generalization of FAs to quasicrystals, which we dubbed Fermi–Bragg arcs due to their close connection with the diffraction spectrum. Although manifested in a particular example, we expect these novel arcs to be universal.

An interesting question for future work would be to explore further the connection between the BPs and FBAs. For example, one could attempt to show the quantized WP charges by integrating the Berry curvature (now defined in Fourier space) flowing through some small sphere surrounding the WP. Even though the diffraction spectrum is dense [38], a finite system sets a finite momentum resolution, and a sufficiently small sphere could be able to resolve the Berry curvature monopoles. This dense character also raises the question of whether it is more appropriate to interpret this system as hosting a Weyl density, with a momentum-dependent (possibly smoothly varying) charge.

Another interesting direction in which to push our model would be in conceptualizing a *fully* quasicrystalline system. To do so, one could for example introduce an Aubry–André-like potential [39] in z, thereby breaking periodicity in all directions. So long as the strength of this potential is not too large, we expect the WPs to remain isolated from bulk bands, and therefore they could be tracked through the quadratic dependence of the DOS, which remains well-defined, as well as extensions of the local Chern marker to 3D [40]. Also, in addition to providing a sensible explanation for the observed WPs in a stack of chalcogenide quasicrystals [24], the robustness and simplicity of the model would allow for an implementation in an photonic or acoustic platform. One could either explicitly break time-reversal through some magnetic mechanism or by employing a tunable parameter as a synthetic time dimension [41–43]. Another alternative is to rely on some crystalline symmetry (e.g., mirror) and force a gap closure through interpolation between phases with distinct invariants associated with such symmetry [44]. Although less robust than our proposal, this would allow a time-reversal invariant implementation, and therefore could be more straightforward.

The authors thank Sachin Vaidya and Aidan Reddy for stimulating discussions and helpful suggestions. A.G.F. acknowledges support from the Henry W. Kendall Fellowship and the Whiteman Fellowship. This research is based upon work supported in part by the Air Force Office of Scientific Research under Grant No. FA9550-20-1-0115 and FA9550-21-1-0299, the U.S. Office of Naval Research (ONR) Multidisciplinary University Research Initiative (MURI) Grant No. N00014-20-1-2325 on Robust Photonic Materials with High-Order Topological Protection, and the U.S. Army Research Office through the Institute for Soldier Nanotechnologies at MIT under Collaborative Agreement No. W911NF-18-2-0048. The

MIT SuperCloud and Lincoln Laboratory Supercomputing Center provided computing resources that contributed to the results reported in this work.

[1] M. Z. Hasan and C. L. Kane, Colloquium: Topological insulators, Rev. Mod. Phys **82**, 3045 (2010).

[2] N. R. Cooper, J. Dalibard, and I. B. Spielman, Topological bands for ultracold atoms, Rev. Mod. Phys. **91**, 015005 (2019).

[3] L. Lu, J. D. Joannopoulos, and M. Soljačić, Topological photonics, Nat. Photonics **8**, 821 (2014).

[4] T. Ozawa, H. M. Price, A. Amo, N. Goldman, M. Hafezi, L. Lu, M. C. Rechtsman, D. Schuster, J. Simon, and O. Zilberberg, Topological photonics, Rev. Mod. Phys **91**, 015006 (2019).

[5] G. Ma, M. Xiao, and C. T. Chan, Topological phases in acoustic and mechanical systems, Nat. Rev. Phys. **1**, 281 (2019).

[6] P. Delplace, J. B. Marston, and A. Venaille, Topological origin of equatorial waves, Science **358**, 1075 (2017).

[7] K. V. Klitzing, G. Dorda, and M. Pepper, New method for high-accuracy determination of the fine-structure constant based on quantized Hall resistance, Phys. Rev. Lett. **45**, 494 (1980).

[8] D. J. Thouless, M. Kohmoto, M. P. Nightingale, and M. den Nijs, Quantized Hall conductance in a two-dimensional periodic potential, Phys. Rev. Lett. **49**, 405 (1982).

[9] B. A. Bernevig, T. L. Hughes, and S.-C. Zhang, Quantum spin Hall effect and topological phase transition in HgTe quantum wells, Science **314**, 1757 (2006).

[10] M. König, S. Wiedmann, C. Brüne, A. Roth, H. Buhmann, L. W. Molenkamp, X. L. Qi, and S. C. Zhang, Quantum spin Hall insulator state in HgTe quantum wells, Science **318**, 766 (2007).

[11] N. P. Armitage, E. J. Mele, and A. Vishwanath, Weyl and Dirac semimetals in three-dimensional solids, Rev. Mod. Phys. **90**, 015001 (2018).

[12] S. Y. Xu, I. Belopolski, N. Alidoust, M. Neupane, G. Bian, C. Zhang, R. Sankar, G. Chang, Z. Yuan, C. C. Lee, *et al.*, Discovery of a Weyl fermion semimetal and topological Fermi arcs, Science **349**, 613 (2015).

[13] L. Lu, Z. Wang, D. Ye, L. Ran, L. Fu, J. D. Joannopoulos, and M. Soljačić, Experimental observation of Weyl points, Science **349**, 622 (2015).

[14] G. E. Volovik, *The Universe in a Helium Droplet* (Clarendon Press, Oxford, 2003).

[15] X. Wan, A. M. Turner, A. Vishwanath, and S. Y. Savrasov, Topological semimetal and Fermi-arc surface states in the electronic structure of pyrochlore iridates, Phys. Rev. B **83**, 205101 (2011).

[16] C. Guo, V. S. Asadchy, B. Zhao, and S. Fan, Light control with Weyl semimetals, arXiv:2209.00701 (2022).

[17] R. Bianco and R. Resta, Mapping topological order in coordinate space, Phys. Rev. B **84**, 241106 (2011).

[18] T. A. Loring and M. B. Hastings, Disordered topological insulators via C^*-algebras, EPL **92**, 67004 (2011).

[19] A. Kitaev, Anyons in an exactly solved model and beyond, Ann. Phys. (N.Y.) **321**, 2 (2006).

[20] J. Fan and H. Huang, Topological states in quasicrystals, Front. Phys **17**, 13203 (2022).

[21] A. Agarwala and V. B. Shenoy, Topological insulators in amorphous systems, Phys. Rev. Lett. **118**, 236402 (2017).

[22] A. Cerjan and T. A. Loring, An operator-based approach to topological photonics, arXiv:2209.04533 (2022).

[23] R. Penrose, The role of aesthetics in pure and applied mathematical research, Bull. Inst. Math. Appl. **10** (1974).

[24] J. D. Cain, A. Azizi, M. A. Conrad, S. M. Griffin, and A. Zettl, Layer-dependent topological phase in a two-dimensional quasicrystal and approximant, PNAS **117**, 26135 (2020).

[25] N. G. de Bruijn, Algebraic theory of Penrose's non-periodic tilings of the plane. i, Indagationes Math. (Proc.) **84**, 39 (1981).

[26] H. Tsunetsugu, T. Fujiwara, K. Ueda, and T. Tokihiro, Electronic properties of the Penrose lattice. I. Energy spectrum and wave functions, Phys. Rev. B **43**, 15 (1991).

[27] X.-L. Qi, Y.-S. Wu, and S.-C. Zhang, Phys. Rev. B **74**, 085308 (2006).

[28] M. D. Caio, G. Möller, N. R. Cooper, and M. J. Bhaseen, Topological marker currents in Chern insulators, Nat. Phys. **15**, 257 (2019).

[29] L. Ulčakar, J. Mravlje, and T. Rejec, Kibble–Zurek behavior in disordered Chern insulators, Phys. Rev. Lett. **125**, 216601 (2020).

[30] T. Chalopin, T. Satoor, A. Evrard, V. Makhalov, J. Dalibard, R. Lopes, and S. Nascimbene, Probing chiral edge dynamics and bulk topology of a synthetic Hall system, Nat. Phys. **10**, 1017 (2020).

[31] D.-T. Tran, A. Dauphin, N. Goldman, and P. Gaspard, Topological Hofstadter insulators in a two-dimensional quasicrystal, Phys. Rev. B **91**, 85125 (2015).

[32] D. Vanderbilt, *Berry Phases in Electronic Structure Theory* (Cambridge University Press, Cambridge, 2018).

[33] H. B. Nielsen and M. Ninomiya, Absence of neutrinos on a lattice: (i). proof by homotopy theory, Nucl. Phys. B **185**, 20 (1981).

[34] H. B. Nielsen and M. Ninomiya, Absence of neutrinos on a lattice: (II). Intuitive topological proof, Nucl. Phys. B **193**, 173 (1981).

[35] W. Man, M. Megens, P. J. Steinhardt, and P. M. Chaikin, Experimental measurement of the photonic properties of icosahedral quasicrystals, Nature **436**, 993 (2005).

[36] C. Wang, F. Liu, and H. Huang, Effective model for fractional topological corner modes in quasicrystals, Phys. Rev. Lett. **129**, 056403 (2022).

[37] S. Spurrier and N. R. Cooper, Theory of quantum oscillations in quasicrystals: Quantizing spiral Fermi surfaces, Phys. Rev. B **100**, 081405 (2019).

[38] D. Levine and P. J. Steinhardt, Quasicrystals. I. Definition and structure, Phys. Rev. Lett. **8**, 15 (1986).

[39] S. Aubry and G. André, Analyticity breaking and Anderson localization in incommensurate lattices, Ann. Isr. Phys. Soc. **3**, 18 (1980).

[40] J. Sykes and R. Barnett, Local topological markers in odd dimensions, Phys. Rev. B **103**, 155134 (2021).

[41] F. Lederer, G. I. Stegeman, D. N. Christodoulides, G. Assanto, M. Segev, and Y. Silberberg, Discrete solitons in optics, Physics Reports **463**, 1 (2008).

[42] M. C. Rechtsman, J. M. Zeuner, Y. Plotnik, Y. Lumer, D. Podolsky, F. Dreisow, S. Nolte, M. Segev, and A. Szameit, Photonic Floquet topological insulators, Nature **496**, 196 (2013).

[43] M. A. Bandres, M. C. Rechtsman, and M. Segev, Topological photonic quasicrystals: Fractal topological spectrum and protected transport, Phys. Rev. X **6**, 011016 (2016).

[44] L. Fu, Topological crystalline insulators, Phys. Rev. Lett. **106**, 106802 (2011).